Supplementary materials

Table S1. The experimental bond lengths [Å] and angles [°] for **1-6**.

Table S2. The comparison of the experimental and optimized bond lengths [Å] for three DFT method (B3LYP, BP86, PBE1PBE) combined with several basis sets.

Table S3. The energy and molar absorption coefficients of experimental absorption bands and the electronic transitions calculated with the TDDFT method for **1**.

Table S4. The energy and molar absorption coefficients of experimental absorption bands and the electronic transitions calculated with the TDDFT method for **3**.

Figure S1. The experimental and calculated (non-scaled) vibrational spectra of **1** and **3**.

Figure S2. ^{1}H NMR spectra of **1**a and **3**

Figure S3. Difference in the bond distance Re–N_{imido} between calculated values and the crystallographic results obtained by employing B3LYP, BP86, PBE1PBE method for *trans*-(Cl,Cl)-[Re(*p*-$NC_6H_4CH_3$)Cl_2(py-2-COO)(PPh_3)] (a) and *cis*-(Cl,Cl)-[Re(*p*-$NC_6H_4CH_3$)Cl_2(py-2-COO)(PPh_3)] (b).

Figure S4. The contours of natural bond orbitals (NBOs) between the rhenium and the *p*-tolylimido ligand for **1** (a) and **3** (b).

Table S1. The experimental bond lengths [Å] and angles [°] for **1-6**.

	1a (X = Cl)	**1b** (X = Cl)	**2** (X = Br)	**3** (X = Cl)	**4** (X = Br)	**5** (X = Cl)	**6** (X = Br)
Bond lengths							
Re(1)-N(2)	1.708(6)	1.650(17)	1.708(11)	1.708(4)	1.717(3)	1.747(3)	1.746(4)
Re(1)-O(1)	2.035(6)	2.027(10)	2.076(9)	2.072(3)	2.057(3)	1.915(3)	1.900(3)
Re(1)-N(1)	2.156(8)	2.151(7)	2.124(10)	2.110(3)	2.113(4)		
Re(1)-X(1)	2.389(2)	2.391(3)	2.5401(16)	2.3571(11)	2.5120(6)	2.4550(10)	2.6052(7)
Re(1)-X(2)	2.420(3)	2.405(3)	2.5497(14)	2.3928(12)	2.5490(6)	2.4006(9)	2.5490(7)
Re(1)-P(1)	2.433(2)	2.450(2)	2.450(3)	2.4398(11)	2.4444(11)	2.4936(10)	2.5050(13)
Re(1)-P(2)						2.4979(11)	2.5112(13)
Bond angles							
N(2)-Re(1)-O(1)	172.1(3)	172.2(5)	172.2(5)	168.39(12)	168.39(13)	172.20(12)	171.23(19)
N(2)-Re(1)-N(1)	100.5(3)	96.0(5)	96.6(5)	96.36(14)	94.76(15)		
O(1)-Re(1)-N(1)	75.6(3)	76.7(3)	75.6(3)	75.66(11)	75.45(13)		
N(2)-Re(1)-X(1)	101.1(2)	98.0(4)	94.8(3)	98.65(11)	99.49(12)	89.18(9)	87.88(16)
O(1)-Re(1)-X(1)	85.8(2)	84.3(2)	84.1(2)	90.28(7)	90.76(8)	83.07(8)	84.09 (12)

N(1)-Re(1)-X(1)	88.2(2)	85.7(2)	86.7(3)	163.91(9)	165.23(10)		
N(2)-Re(1)-X(2)	91.3(2)	94.6(4)	96.5(4)	102.73(12)	98.95(12)	101.94(9)	100.44(16)
O(1)-Re(1)-X(2)	81.5(2)	82.5(2)	83.7(2)	84.84(8)	86.37(8)	85.82(8)	87.84(12)
N(1)-Re(1)-X(2)	84.1(2)	86.8(2)	84.6(3)	82.79(9)	83.80(9)		
X(1)-Re(1)-X(2)	166.47(9)	165.95(10)	166.45(5)	88.27(4)	90.14(2)	168.87(4)	170.79(2)
N(2)-Re(1)-P(1)	96.9(2)	92.9(5)	93.1(4)	93.25(12)	93.98(12)	90.58(10)	91.21(15)
O(1)-Re(1)-P(1)	87.14(18)	94.3(3)	94.6(2)	79.37(8)	80.80(9)	89.23(8)	86.73(10)
N(1)-Re(1)-P(1)	162.6(2)	170.7(2)	169.9(3)	95.59(9)	94.51(10)		
X(1)-Re(1)-P(1)	88.53(8)	95.72(12)	89.82(9)	89.33(4)	88.38(3)	94.93(4)	98.60(4)
X(2)-Re(1)-P(1)	95.47(10)	89.83(9)	96.98(10)	164.02(4)	167.06(3)	85.59(3)	85.32(4)
C(25)-N(2)-Re(1)	167.9(6)	171.9(10)	173.1(10)	174.4(3)	175.1(3)		
O(1)-Re(1)-P(2)						91.19(8)	87.00(10)
N(2)-Re(1)-P(2)						89.44(10)	96.03(15)
P(1)-Re(1)-P(2)						176.80(3)	171.45(4)
P(2)-Re(1)-X(2)						91.27(3)	88.64(4)
P(2)-Re(1)-X(1)						88.27(4)	86.52(4)
C(37)-N(2)-Re(1)						161.5(3)	161.1(4)

Table S2. The comparison of the experimental and optimized bond lengths [Å] for three DFT methods (B3LYP, B3LYP^{d}, BP86, PBE1PBE) combined with several basis sets.

1														
Bond	X-Ray	B3LYP				B3LYP [d]	BP86				PBE1PBE			
		LTZ631	LTZ631+	LTZ6311	LDZ631+	LDZ631+	LTZ631	LTZ631+	LTZ6311	LDZ631+	LTZ631	LTZ631+	LTZ6311	LDZ631+
Re(1)-N(1)	2.156(8)	2.147	2.145	2.146	2.146	2.146	2.114	2.110	2.111	2.112	2.122	2.121	2.121	2.121
Re(1)-N(2)	1.708(6)	1.720	1.719	1.720	1.720	1.714	1.741	1.739	1.739	1.739	1.707	1.707	1.707	1.706
Re(1)-O(1)	2.035(6)	2.017	2.025	2.024	2.025	2.033	2.009	2.017	2.017	2.020	2.010	2.016	2.016	2.018
Re(1)-P(1)	2.433(2)	2.490	2.496	2.498	2.493	2.431	2.478	2.483	2.483	2.479	2.446	2.451	2.451	2.448
Re(1)-Cl(1)	2.389(2)	2.444	2.434	2.434	2.434	2.434	2.422	2.419	2.419	2.420	2.406	2.399	2.401	2.406
Re(1)-Cl(2)	2.420(3)	2.457	2.457	2.454	2.458	2.449	2.451	2.443	2.442	2.444	2.421	2.420	2.418	2.413

3														
Bond	X-Ray	B3LYP				B3LYP [d]	BP86				PBE1PBE			
		LTZ631	LTZ631+	LTZ6311	LDZ631+	LDZ631+	LTZ631	LTZ631+	LTZ6311	LDZ631+	LTZ631	LTZ631+	LTZ6311	LDZ631+
Re(1)-N(1)	2.110(3)	2.142	2.142	2.144	2.142	2.135	2.104	2.104	2.104	2.104	2.113	2.113	2.114	2.112
Re(1)-N(2)	1.708(4)	1.719	1.718	1.718	1.717	1.715	1.739	1.738	1.738	1.737	1.706	1.705	1.705	1.705
Re(1)-O(1)	2.072(3)	2.041	2.049	2.049	2.051	2.058	2.033	2.040	2.040	2.042	2.035	2.040	2.039	2.042
Re(1)-P(1)	2.4398(11)	2.501	2.508	2.508	2.501	2.434	2.478	2.483	2.483	2.478	2.449	2.454	2.453	2.449
Re(1)-Cl(1)	2.3928(12)	2.417	2.410	2.409	2.413	2.409	2.404	2.395	2.396	2.399	2.382	2.377	2.377	2.379
Re(1)-Cl(2)	2.3571(11)	2.389	2.386	2.386	2.387	2.385	2.382	2.378	2.378	2.379	2.360	2.358	2.398	2.358

B3LYP [d] - B3LYP functional improved by adding dispersion correction

Table S3. The energy and molar absorption coefficients of experimental absorption bands and the electronic transitions calculated with the TDDFT method for **1**.

The most important orbital excitations	Character	λ[nm]	E[eV]	f x10^2	Experimental Λ[nm](E[eV])ε
H→L	d/π(Cl) → π*(p-tol)/d	712.1	1.74	0.04	791.2 (1.57) 130
H→L+1	d/π(Cl) → π*(py-2-COO)/d/π*(p-tol)	606.9	2.04	0.76	602.4 (2.06) 200
H→L+2	d/π(Cl) → π*(py-2-COO)/d/π*(p-tol)	412.6	3.00	8.83	425.6 (2.91) 7400
H-8→L	π(PPh_3)/π(p-tol)/π(Cl) → π*(p-tol)/d	330.2	3.76	13.20	333.2 (3.72) 43 220
H-2→L	π(PPh_3)/π(p-tol) → π*(p-tol)/d	320.0	3.87	26.50	
H-8→L+1	π(PPh_3)/π(p-tol)/π(Cl) → π*(py-2-COO)/d/π*(p-tol)	282.5	4.39	3.24	266.8 (4.65) 44 100
H-8→L+2	π(PPh_3)/π(p-tol)/π(Cl) → π*(py-2-COO)/d/π*(p-tol)	249.5	4.97	7.88	224.8 (5.52) 76 800
H-5→L+2	π(PPh_3)/π(Cl) → π*(py-2-COO)/d/π*(p-tol)	239.6	5.17	6.48	
H-15→L+1	π(py-2-COO)/π(Cl)/d → π*(py-2-COO)/d/π*(p-tol)	236.6	5.24	6.01	

Table S4. The energy and molar absorption coefficients of experimental absorption bands and the electronic transitions calculated with the TDDFT method for **3**.

The most important orbital excitations	Character	λ[nm]	E[eV]	f x10^2	Experimental Λ[nm](E[eV])ε
H→L	d/π(Cl)/π(py-2-COO) → π*(p-tol)/d/π*(py-2-COO)	654.9	1.89	0.19	763.6 (1.62) 155
H→L+1	d/π(Cl)/π(py-2-COO) → π*(py-2-COO)/d/π*(p-tol)	564.4	2.20	0.33	617.6 (2.01) 190
H→L+2	d/π(Cl)/π(py-2-COO)→ π*(py-2-COO)/d/π*(p-tol)	397.5	3.12	0.13	418.0 (2.97) 3 200
H-1→L	π(p-tol)/d/π(Cl) → π*(p-tol)/d/ π*(py-2-COO)	354.5	3.50	9.13	333.6 (3.72) 24 500
H-1→L	π(p-tol)/d/π(Cl) → π*(p-tol)/d/ π*(py-2-COO)	321.4	3.86	35.04	
H-11→L	π(py-2-COO)/π(Cl) → π*(p-tol)/d/ π*(py-2-COO)	256.7	4.83	3.58	260.4 (4.77) 22 270
H-1→L+8	π(p-tol)/d/π(Cl) → π*(p-tol)	223.1	5.56	10.24	223.6 (5.54) 69 420
H-15→L+1	π(Cl)/π(py-2-COO)/π(p-tol) → π*(py-2-COO)/d/π*(p-tol)	219.3	5.65	8.75	

Figures

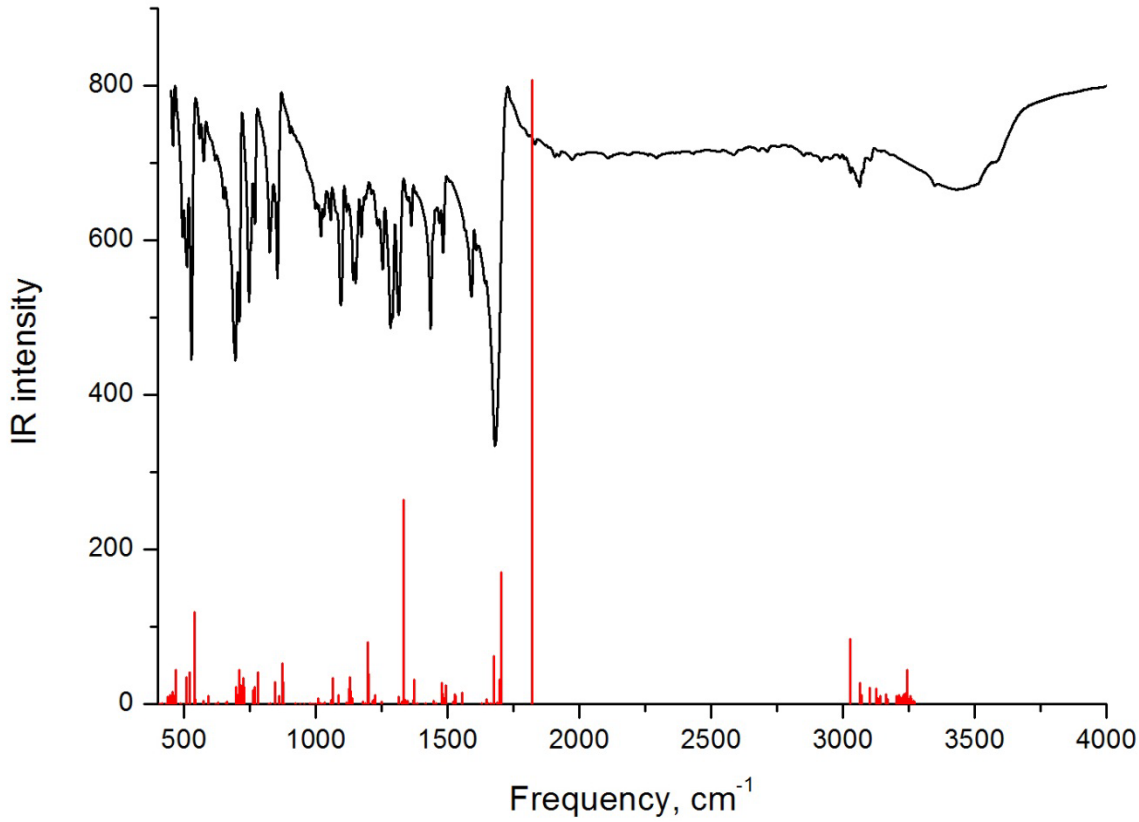
IR intensity
0
200
400
600
800
500
1000
1500
2000
2500
3000
3500
4000
Frequency, cm-1

a)

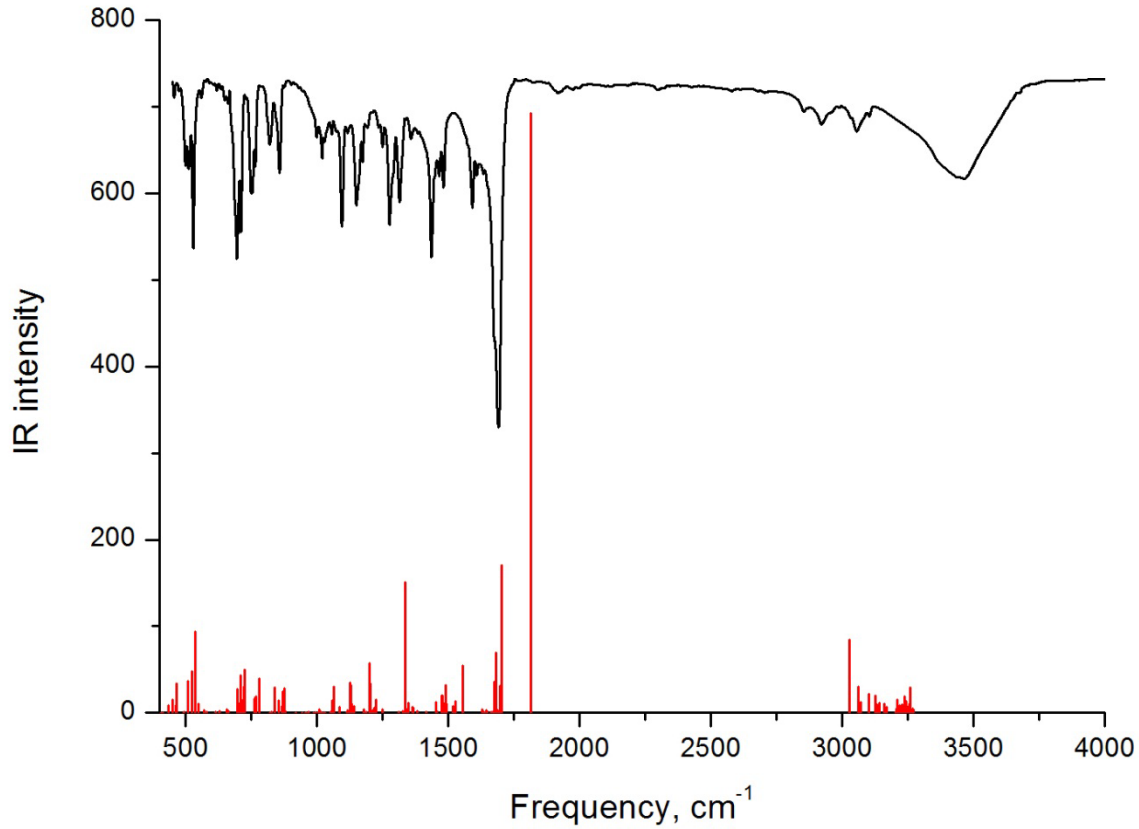
IR intensity
0
200
400
600
800
500
1000
1500
2000
2500
3000
3500
4000
Frequency, cm-1

b)

Figure S1. The experimental and calculated (non-scaled) vibrational spectra of **1a** (a) and **3** (b).

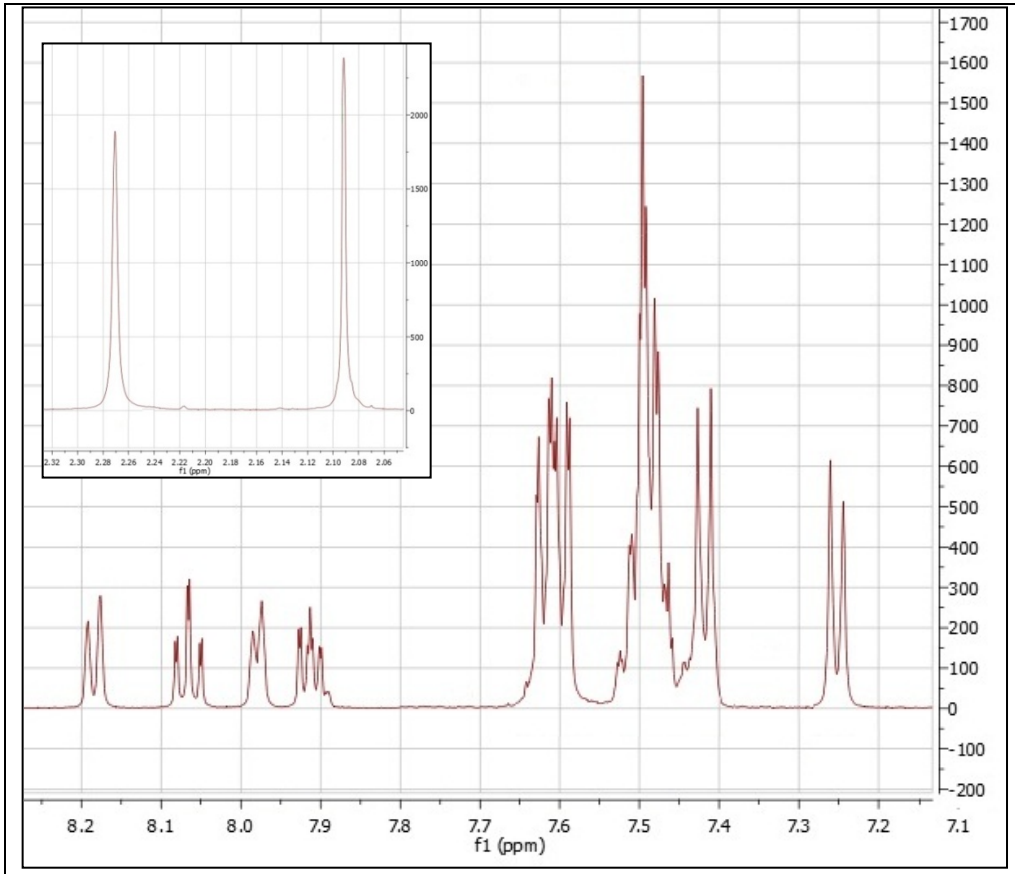

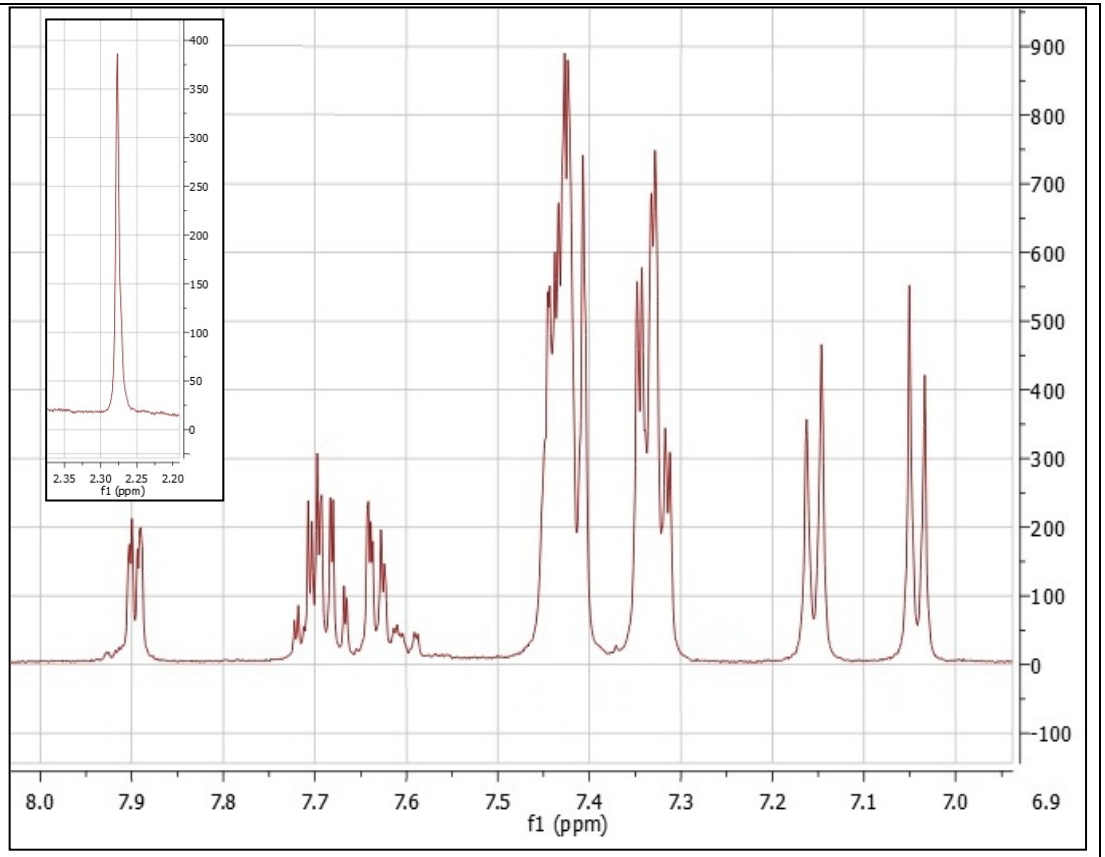

Figure S2. ^{1}H NMR spectra of **1**a and **3**

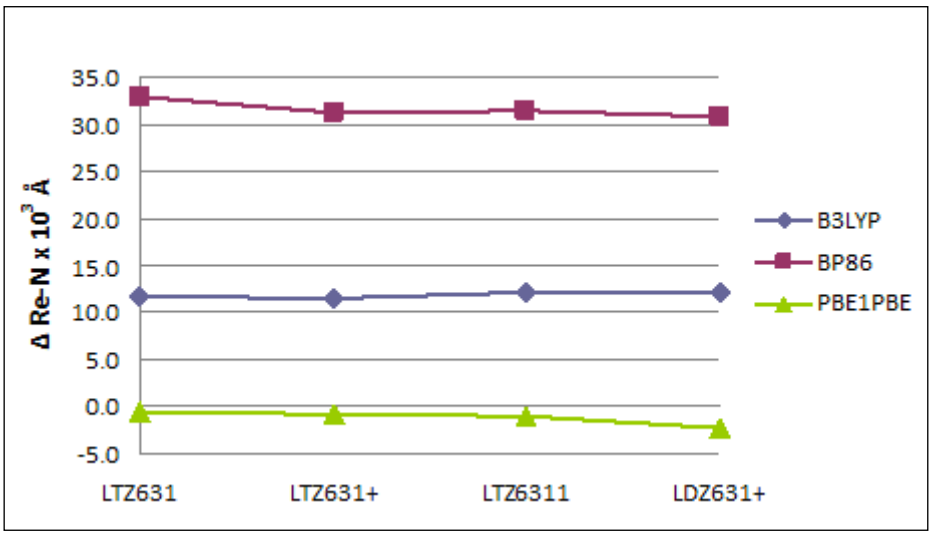

a)

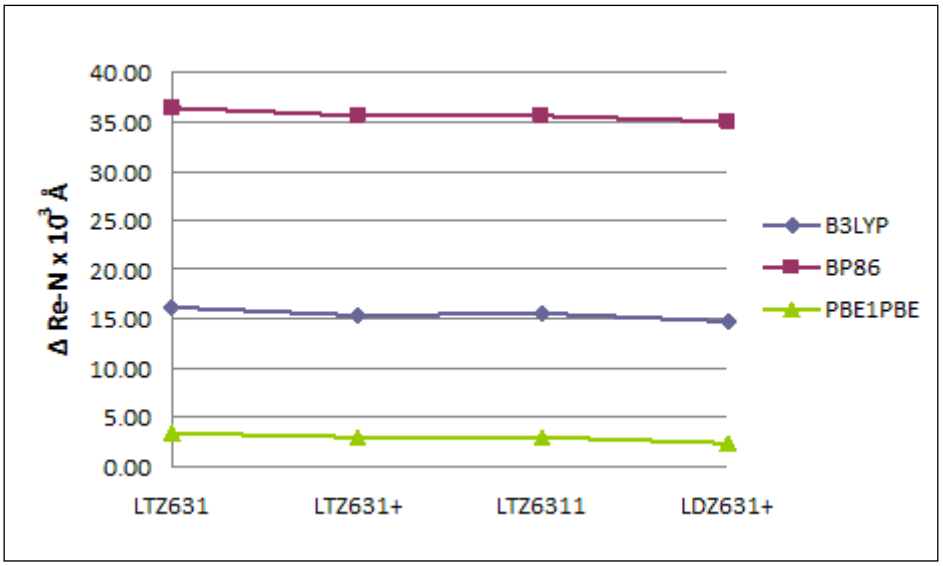

b)

Figure S3. Difference in the bond distance Re–N_{imido} between calculated values and the crystallographic results obtained by employing B3LYP, BP86, PBE1PBE method for *trans*-(Cl,Cl)-[Re(*p*-$NC_6H_4CH_3$)Cl_2(py-2-COO)(PPh_3)] (a) and *cis*-(Cl,Cl)-[Re(*p*-$NC_6H_4CH_3$)Cl_2(py-2-COO)(PPh_3)] (b).

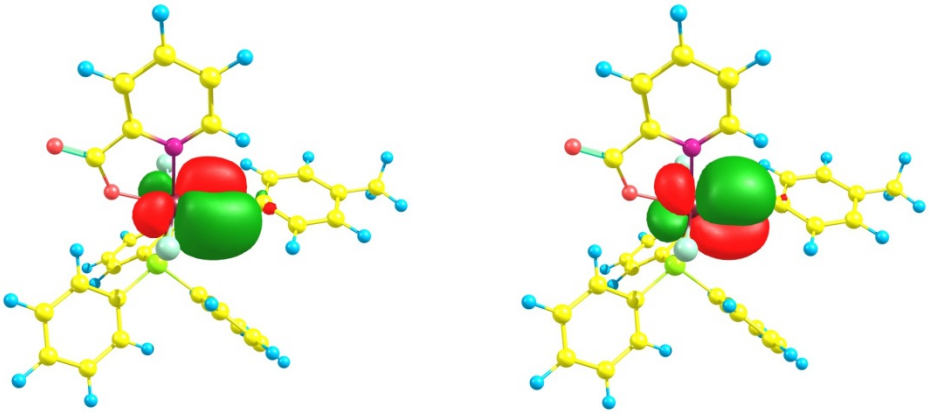

$0.609\ (d)_{Re} + 0.793\ (p)_{N}$ $0.657\ (d)_{Re} + 0.753\ (p)_{N}$

a)

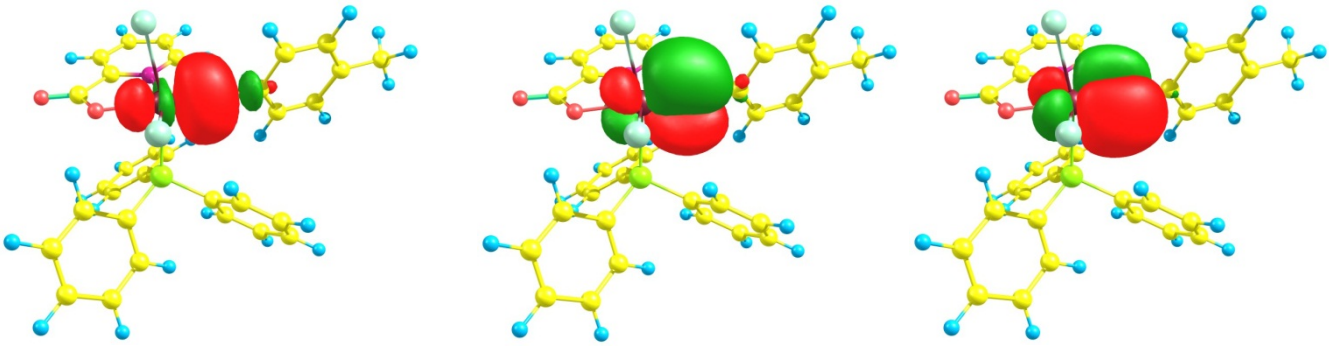

$0.528\ (sp^{0.48}d^{3.39})_{Re} + 0.849(sp^{0.70})_{N}$ $0.617\ (d)_{Re} + 0.787\ (p)_{N}$ $0.635\ (d)_{Re} + 0.772\ (p)_{N}$

b)

Figure S4. The contours of natural bond orbitals (NBOs) between the rhenium and the *p*-tolylimido ligand for **1** (a) and **3** (b).